ISSN 1063-7729, Astronomy Reports, 2008, Vol. 52, No. 3, pp. 226–236. © Pleiades Publishing, Ltd., 2008.
Original Russian Text © Yu.Yu. Balega, V.V. Leushin, M.K. Kuznetsov, V. Tamazian, 2008, published in Astronomicheskiĭ Zhurnal, 2008, Vol. 85, No. 3, pp. 257–267.

Atmospheric Chemical Abundances and the Evolutionary Status of the Spectroscopic and Speckle-Interferometric Binary 9 Cyg

Yu. Yu. Balega[1], V. V. Leushin[1,2], M. K. Kuznetsov[2], and V. Tamazian[3]

[1] *Special Astrophysical Observatory, Russian Academy of Sciences, Nizhniĭ Arkhyz, Karachaĭ-Cherkessian Republic, 357147 Russia*

[2] *Southern Federal University, ul. Bolshaya Sadovaya 105, Rostov-on-Don, 334006 Russia*

[3] *Ramón María Aller Observatory, Santiago de Compostela University, P. O. Box 197, Santiago de Compostela, Spain*

Received May 18, 2007; in final form, June 22, 2007

Abstract—We have performed speckle interferometry with the 6-m telescope of the Special Astrophysical Observatory and spectroscopy (at 3700–9200 Å) with the 2-m telescope at Peak Terskol of the spectroscopic and interferometric binary 9 Cyg, which is a composite-spectrum star with an orbital period of 4.3 yrs. The atmosphere of the system's primary component is analyzed in detail. The luminosities of both components estimated to be $L_1 = 103.8\ L_\odot$, $L_2 = 55.2\ L_\odot$, where $L_\odot$ is the solar luminosity, and their effective temperatures to be $T_e(1) = 5300$ K and $T_e(2) = 9400$ K. The abundances of C, N, O, Fe, and other elements in the primary's atmosphere have been derived. The chemical composition shows signatures of mixing of material from its atmosphere and the region of nuclear reactions. The evolutionary status of 9 Cyg has been determined. The binary's age is about 400 million years; the brighter star is already in the transition to becoming a red giant, while the secondary is still in the hydrogen-burning stage near the zero-age main sequence. We suggest an evolutionary model for the binary's orbit that explains the high eccentricity, $e = 0.79$.

PACS numbers: 97.80.Af, 97.80.Fk, 97.10.Tk, 97.10.Tk
DOI: 10.1134/S1063772908030050

1. INTRODUCTION

Binaries with high orbital eccentricities ($e > 0.6–0.7$) are of interest for theories of the formation and evolution of multiple stars. Their studies provide information about the internal structure of these stars, whose apsidal motion is due primarily to the mass distribution in the volumes of the stars forming the binary.

Studies of high-eccentricity binaries with composite spectra are of special interest. 9 Cyg, a symbiotic system consisting of a G giant and a hot A dwarf, is a typical representative of this stellar family. The spectral classification of 9 Cyg in the literature is very confused due to difficulties in separately determining the spectral types of the hot and cool components using spectra taken mainly at 3800–4800 ÅHynek [1] was the first to suggest based on the absence of hydrogen lines in the spectra that the binary's primary had a very high rotation rate, whereas Markovitz [2] demonstrated that the cool component was an ordinary giant with moderate luminosity. Abt and Levy [3] used Coudé spectroscopy to derive the principal orbital parameters of 9 Cyg, which were later considerably improved by Griffin et al. [4] using radial velocity measurements made in Cambridge. The latter authors found the system's period ($P = 4.303$ years) and eccentricity ($e = 0.7887$), and estimated the masses of the primary and secondary to be $2.9\ M_\odot$ and $2.7\ M_\odot$.

Interferometric observations of symbiotic binaries are crucial for determining the components' masses and luminosities. However, the angular separation between the 9 Cyg components is almost always less than $0.04''$, so that speckle-interferometric observations, even with the largest telescopes, have been at the diffraction resolution limit, and have often turned out to be erroneous. Based on only six interferometric points, Baize [5] suggested an apparent orbit with a period of $P = 4.56$ years and an eccentricity of $e = 0.82$, which should be considered tentative. The most accurate speckle-interferometry measurements with the 6-m telescope of the Special Astrophysical Observatory indicated, along with positional information, that the magnitude difference between the cool and hot components in an 80 Å band at 6560 Å was $\Delta m = 1.31^m$ [6]. Using far-ultraviolet IUE spectra,

Parsons and Ake [7] estimated the hot star's luminosity and derived $\Delta m_V = 1.1$, whereas Griffin et al. [4] computed a photometric model of the binary yielding $\Delta m_V = 0.75$. It is also reported in [8] that the fluxes from the two stars should become comparable near 4000 Å.

Data on the luminosities and spectral types of the 9 Cyg components likewise do not agree well. Most authors quote spectral types for the cool component between F8III and G8III. The usual classification of the hot star in the system is A0V–A2V; in particular, Parsons and Ake [7] derived the spectral type A0 from UV measurements. However, Ginestet and Carquillat [9] find that this star could be an A2III giant as well. Note that spectral types based on UV data are often earlier than those derived from ground-based data, since they are not influenced by the cool components.

The Hipparcos [10] astrometric parallax of 9 Cyg ($\pi_H = 6.06$ milliarcseconds, $d = 165$ pc) has an uncertainty of about 10%, and does not agree well with the luminosity of the binary expected from the standard Schmidt–Kaler calibrations [11]: both components turn out to be too bright by as much as a magnitude.

To estimate the spectral types of the components of 9 Cyg, improve their atmospheric parameters, and determine the binary's evolutionary status, we observed it spectroscopically with the 2-m telescope at Peak Terskol in a wide spectral range between 3500 and 9600 Å. This paper presents our reductions of the spectra and the resulting model of the symbiotic binary. Using 9 Cyg as an example, we also discuss one of the possible formation scenarios for binaries with rapidly rotating hot components.

2. OBSERVATIONS AND REDUCTIONS

We obtained spectra of 9 Cyg on October 22 and 23, 2003 using the echelle spectrograph of the 2-m telescope of the International Center for Astronomical, Medical, and Ecologic Studies at Peak Terskol [12] (currently the Terskol Branch of the Institute of Astronomy, Russian Academy of Sciences) with a 1242 × 1152-pixel Write CCD camera (UK). On each of the two nights, we made two one-hour exposures of the star, at 18^h41^m and19^h42^m on October 22, 2003, and at 18^h42^m and 19^h43^m on October 23, 2003, at 3500–9600 Å with a spectral resolution of $R = 45\,000$. After summing the two exposures for the individual nights, we achieved a signal-to-noise ratio of about 200 for the spectra. We reduced the spectral data using the DECH20 software package developed at the Special Astrophysical Observatory [13].

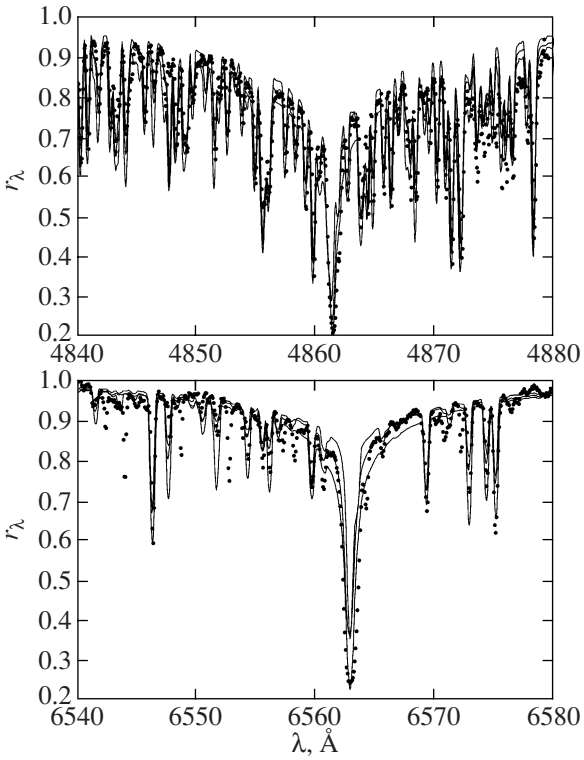

Fig. 1. Observed (points) profiles of the Hα and Hβ lines together with the combined synthetic spectra of the two components calculated for models with the parameters from Table 2. The curves in the top and bottom panels are the spectra for the models with the parameters in the top and bottom parts of Table 2.

Our spectra agree best with that of a G8III late-type giant. No hydrogen lines from the hot component are visible in the spectra, confirming its high rotation rate ($v \sin i > 200$ km/s).

3. GENERAL PARAMETERS OF THE COMPONENTS AND CHARACTERISTICS OF THEIR ATMOSPHERES

3.1. Effective Temperatures

To estimate the effective temperatures of the binary components, we compared theoretically calculated

Table 1. Spectral types and effective temperatures of the components

Reference	Sp(1)	Sp(2)	$T_{eff,1}$, K	$T_{eff,2}$, K
Griffin et al. [4]	G8III	A2V	4560	9150
Martin et al. [8]	F8III	A0V	6050	9595
Parsons and Ake [7]	F8–G8III	A0V	5500	9600

Table 2. Parameters of model atmospheres for the components of 9 Cyg

Component	T_{eff}, K	$\log g$	$H_\lambda(1)/H_\lambda(2)$	V_t, km s^{-1}	$v \sin i$, km s^{-1}
1	4630	2.30	3.34–2.00	2.47	13.0
2	9140	3.74		2.0	200
1	5300	2.30	3.34–2.00	2.47	13.0
2	9400	3.95		2.0	200
1	5500	2.80	3.34–2.00	2.47	13.0
2	9400	3.95		2.0	200

hydrogen-line profiles to the observations. The calculations were performed for model atmospheres with temperatures between 4560 and 6050 K for the primary and between 9150 and 9600 K for the secondary, in agreement with published data on the components' spectral types and the corresponding effective temperatures (Table 1).

Figure 1 compares the observed Hα and Hβ profiles to the combined theoretical synthetic spectra calculated using the SintVA code [14] and LLmodels [15]. The parameters of the three sets of models used to calculate the profiles are given in Table 2; the middle set is closest to the observed profile, while the others demonstrate significant deviations.

The continuum flux ratio of the components ($H_\lambda(1)/H_\lambda(2)$) varies with wavelength, and we assumed $H_\lambda(1)/H_\lambda(2) = 3.34$ when computing the combined spectrum (coming from the two components) near Hα and $H_\lambda(1)/H_\lambda(2) = 2.00$ near Hβ, in agreement with estimates from the magnitude differences. We estimated the surface gravities of the stars ($\log g$) from their masses [4] ($M_1 = 2.9\ M_\odot$ and $M_2 = 2.7\ M_\odot$) and the radii corresponding to their luminosities and temperatures. We used the parallax of [8] to find the luminosities, which differs from the Hipparcos parallax [10] by less than 10%, but is in better agreement with the positions of the components on the isochrones of their evolutionary tracks (see below).

Unfortunately, we are not able to achieve a full agreement between the theoretical and observed profiles, but can conclude from the coincidence of the hydrogen-line wings that the atmospheric parameters of the components are close to $T_{eff} = 5300 \pm 200$ K and $\log g = 2.80 \pm 0.10$ for component 1 and $T_{eff} = 9400 \pm 200$ K and $\log g = 3.95 \pm 0.10$ for component 2, for solar abundances (i.e., $z = 0.019$). A temperature change by 200 K leads to significant differences between the theoretical and observed hydrogen-line profiles; at the same time, luminosity differences due to parallax uncertainties lead to the same changes, by 200 K in the temperature and ± 0.10 in the surface gravity. In addition, calculations of the atmospheric iron abundance demonstrate that the ionization equilibrium condition for FeI and FeII, which is violated for other temperatures, is satisfied within the errors for $T_{eff} = 5300$ K. With all this in mind, we take the temperature uncertainties to be within ± 200 K and the uncertainties in the surface gravity to be within ± 0.10. Note that our choice of temperatures is close to the mean of various values derived from the spectral type.

Table 3. Ratios of the squared radii of the components at various wavelengths

λ, Å	$H_\lambda(1)$ ($T_{eff} = 5300$ K, $\log g = 2.80$)	$H_\lambda(2)$ ($T_{eff} = 9400$ K, $\log g = 3.95$)	Δm	R_1^2/R_2^2
4000	9.54×10^6	1.10×10^8	0	11.5
5500	7.00×10^6	4.50×10^7	1.10	17.7
6560	5.43×10^6	2.60×10^7	1.31	16.0

3.2. Radius and Luminosity Ratios for the Components

We can use the brightness differences between the components and our derived effective atmospheric temperatures to estimate the ratios of the components' radii. We selected from the model-atmosphere calculations the light fluxes per cm^2 of surface for wavelengths with known magnitude differences (H_λ). For the star's measured fluxes, $\Delta m = 2.5 \log(H_\lambda(1) R_1^2 / H_\lambda(2) R_2^2)$, and we can use this relation to find R_1^2/R_2^2 (Table 3).

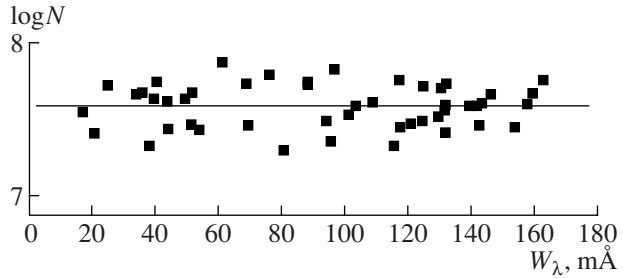

Fig. 2. Iron abundances derived from FeI lines as functions of the equivalent widths of the corresponding lines. The data were obtained for a microturbulence velocity of 2.47 km/s.

The scatter of these results is large. However, if the components' equal brightness indicated by the study of Parsons and Ake [7] ($\Delta m = 0$) shifts in the transition from 4000 to 3700 Å, the ratio R_1^2/R_2^2 becomes 14.1. At the same time, according to various studies (see above), Δm at 5500 Å (V band) varies from 0.645^m to 1.10^m, so that estimates of R_1^2/R_2^2 can vary from 11.6 to 17.7. So, the value $\Delta m = 1.31$ for $\lambda = 6550$ Å determined earlier from observations with the 6-m telescope [6] seems the most accurate, suggesting that R_1^2/R_2^2 is close to 16.0 and $R_1/R_2 = 4$, especially since this value lies within the above admissible range.

Using this radius ratio for the binary components and the most probable effective temperatures, we obtain the luminosity ratio

$$L_1/L_2 = T_1^4 R_1^2/T_2^4 R_2^2 = 1.88.$$

3.3. Iron Abundance and Microturbulence Velocity in the Cool Component's Atmosphere

To determine the iron abundance, we measured the equivalent widths of 48 FeI lines and 23 FeII lines in the spectrum of 9 Cyg 1. These equivalent widths were derived via the component-brightness ratio, $l = E_{\lambda 2}/E_{\lambda 1}$, and the widths observed in the combined spectrum, using the relation $W_{\lambda 1} = W_{\lambda 1,obs}(1 + l)$, where l varies with wavelength between 0.5 and 0.25. No lines of the secondary are visible in the spectrum due to its high rotation rate ($v \sin i = 200$ km/s). The FeI equivalent widths, along with the atomic parameters and $\log N(\mathrm{Fe})$ values for each line derived assuming $V_t = 2.47$ km/s, are presented in Table 4.

Our computations were made with the KONTUR code [16] for models with $T_{eff} = 5300$, $\log g = 2.80$, and various microturbulence velocities. Using the

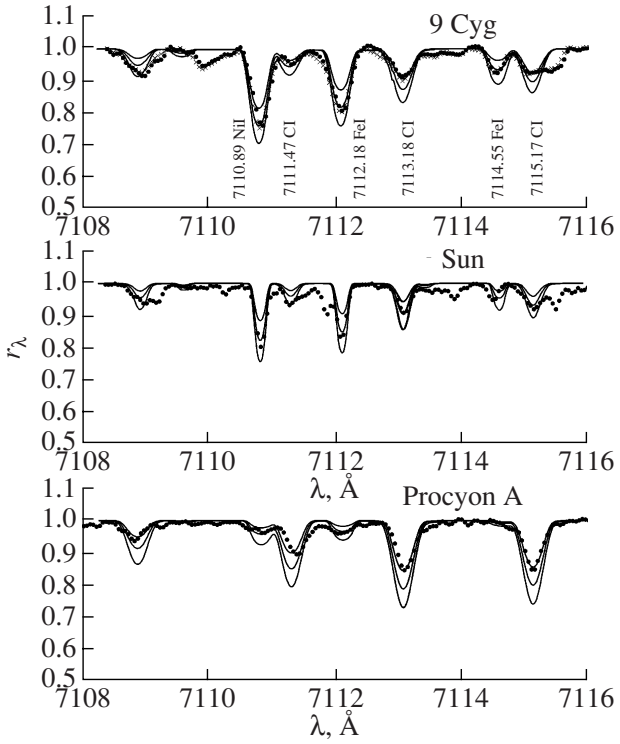

Fig. 3. Observed parts of the spectrum with CI lines (the points and crosses show the spectra on October 22 and 23, 2003) compared to synthetic spectra calculated for 9 Cyg, the Sun, and Procyon A. The middle curve of the synthetic spectrum was calculated for the elemental abundances from Table 6, and the top and bottom curves for those abundances ±0.3 dex.

$\log N(\mathrm{Fe})$ values for various V_t values, we obtained the linear regression fits

$$\log N(\mathrm{Fe}) = \log N(\mathrm{Fe})_0 + kW_\lambda,$$

enabling us to choose a realistic V_t for the stellar atmosphere. The corresponding fits show the microturbulence velocity in the atmosphere of 9 Cyg 1 to be close to 2.47 km/s (Fig. 2).

Table 5 presents equivalent widths for lines of ionized iron, FeII, and the corresponding $\log N(\mathrm{Fe})$ values for the atmosphere of 9 Cyg 1. The mean atmospheric iron abundance 9 Cyg 1 based on the FeI lines is

$$\log N(\mathrm{Fe}) = 7.56 \pm 0.02,$$

and that from FeII lines,

$$\log N(\mathrm{Fe}) = 7.49 \pm 0.07.$$

The rms errors of the means describe the internal accuracy of the results, which agree within the uncertainties. Thus, the atmospheric iron abundance of 9 Cyg 1 essentially coincides with the solar abundance ($\log N(\mathrm{Fe})_\odot = 7.50$) [17].

Table 4. Parameters and equivalent widths of FeI lines and the iron abundance in the atmosphere of 9 Cyg 1 derived from each line

λ, Å	ε_i, eV	$\log gf$	W_λ, mÅ	$\log N$(Fe)	λ, Å	ε_i, eV	$\log gf$	W_λ, mÅ	$\log N$(Fe)
4389.24	0.05	−5.28	95.7	7.35	6265.13	2.18	−2.55	158.0	7.60
4445.47	0.09	−5.44	80.8	7.30	6271.28	3.33	−2.70	51.5	7.47
5044.21	2.85	−2.06	121.0	7.47	6280.62	0.86	−4.39	131.8	7.56
5247.05	0.09	−4.95	143.8	7.61	6297.79	2.22	−2.74	142.0	7.59
5250.21	0.12	−4.94	146.4	7.67	6322.68	2.59	−2.43	130.0	7.52
5253.46	3.28	−1.57	115.8	7.33	6481.87	2.28	−2.98	130.9	7.71
5329.99	4.08	−1.19	104.0	7.59	6498.94	0.96	−4.70	117.5	7.76
5412.78	4.43	−1.72	43.8	7.62	6574.23	0.99	−5.00	88.7	7.73
5491.83	4.19	−2.19	33.7	7.67	6581.21	1.48	−4.68	76.2	7.80
5525.54	4.23	−1.08	94.6	7.49	6593.87	2.43	−2.42	163.1	7.76
5661.35	4.28	−1.76	44.0	7.44	6609.11	2.56	−2.69	132.6	7.74
5701.54	2.56	−2.13	142.7	7.46	6625.02	1.01	−5.34	38.2	7.33
5705.46	4.30	−1.36	69.8	7.46	6667.71	4.58	−2.11	24.7	7.73
5778.45	2.59	−3.44	69.1	7.74	6699.14	4.59	−2.10	16.9	7.55
5784.66	3.40	−2.53	54.0	7.43	6739.52	1.56	−4.79	51.6	7.68
5855.08	4.61	−1.48	49.3	7.64	6750.15	2.42	−2.61	139.6	7.59
5956.69	0.86	−4.60	125.2	7.72	6793.26	4.08	−2.33	35.7	7.68
6082.71	2.22	−3.59	97.0	7.83	6804.27	4.58	−1.81	40.4	7.75
6136.99	2.20	−2.95	117.8	7.45	6837.01	4.59	−1.69	39.4	7.64
6151.62	2.18	−3.30	101.6	7.54	6854.82	4.59	−1.93	20.4	7.41
6173.34	2.22	−2.88	132.3	7.60	6945.20	2.42	−2.44	159.5	7.67
6200.31	2.61	−2.44	124.8	7.49	6971.93	3.02	−3.30	61.5	7.88
6219.28	2.20	−2.43	153.9	7.45	6978.85	2.48	−2.48	132.1	7.41
6240.65	2.22	−3.23	109.2	7.61	7189.15	3.07	−2.77	88.8	7.75

3.4. C, N, and O Atmospheric Abundances for the Cool Component

The C, N, and O line intensities in the spectra of stars with effective temperatures below the solar value ($T_{eff} = 5300$ K for 9 Cyg 1) are very low, and virtually all of these lines are blended with lines of other elements, predominantly FeI lines. This makes C, N, and O abundance determinations from equivalent widths difficult for these stars and subject to considerable uncertainties. Our abundance determinations for 9 Cyg 1 were based on synthetic-spectrum computations in the regions of CI, NI, and OI lines. For comparison, we simultaneously also calculated synthetic spectra for the same spectral regions for the Sun and Procyon A. The observed spectra of the Sun and Procyon A were obtained using the same spectrograph and telescope as the spectra of 9 Cyg.

The characteristics of the stellar models are presented in Table 6.

We selected line parameters from the VALD database [18]. Spectral-line broadening mechanisms were taken into account using the technique described in [19]. The observed and calculated spectra for regions with CI, NI, and OI lines are shown in Figs. 3–5. Table 7 presents the line parameters used to calculate the parts of the synthetic spectrum used to derive the C abundance, together with the elemental abundances derived from these lines.

We made comparisons with the Sun and Procyon A for all parts of the synthetic spectra. Figures 3–5 show the observed spectra (points) together with theoretical calculated curves for three abundances: $\log N = \log N_0 + \Delta \log N$, with $\Delta \log N = -0.3, 0, +0.3$, where $\log N_0$ is the value from Table 6; i.e., for abundances half, equal to, and twice the value for the given model atmosphere. The calculated line profiles fit the observations well, making it possible to estimate the abundances of each of the elements. The resulting mean carbon abundances are

$$\log N(\mathrm{C})_\odot = 8.46 \pm 0.07,$$
$$\log N(\mathrm{C})_{\alpha\ \mathrm{CMi}} = 8.57 \pm 0.10,$$
$$\log N(\mathrm{C})_{9\ \mathrm{Cyg}\ 1} = 8.28 \pm 0.05.$$

Tables 8 and 9 present data analogous to those in Table 6 for nitrogen and oxygen. We found the mean nitrogen abundances to be

$$\log N(\mathrm{N})_\odot = 7.78 \pm 0.06,$$
$$\log N(\mathrm{N})_{\alpha\ \mathrm{CMi}} = 8.15 \pm 0.03,$$
$$\log N(\mathrm{N})_{9\ \mathrm{Cyg}\ 1} = 8.21 \pm 0.10$$

and the mean oxygen abundances to be

$$\log N(\mathrm{O})_\odot = 8.96 \pm 0.10,$$
$$\log N(\mathrm{O})_{\alpha\ \mathrm{CMi}} = 9.06 \pm 0.10,$$
$$\log N(\mathrm{O})_{9\ \mathrm{Cyg}\ 1} = 8.74 \pm 0.10.$$

A comparison of our solar abundances with those published earlier indicates agreement within the uncertainties for carbon and nitrogen:

$$\log N(\mathrm{C})_\odot = 8.46 \pm 0.07 \quad \text{(our value)}$$
$$\text{and} \quad 8.46 \pm 0.07\ [20],$$
$$\log N(\mathrm{N})_\odot = 7.78 \pm 0.06 \quad \text{(our value)}$$
$$\text{and} \quad 7.83 \pm 0.11\ [20].$$

The oxygen abundances also coincide with earlier data calculated without non-LTE effects:

$$\log N(\mathrm{O})_\odot = 8.96 \pm 0.10 \quad \text{(our determination)}$$
$$\text{and} \quad 8.93 \pm 0.04\ [20].$$

At the same time, estimates derived taking into account non-LTE effects give solar abundances that are lower by 0.3 dex [22]. Thus, we consider the differences of the C and N abundances for the atmospheres of the Sun and 9 Cyg 1 we have found to be real. Taking into account non-LTE effects should make our oxygen abundances lower for the Sun as well as for 9 Cyg 1. On the other hand, the atmospheric oxygen abundance for 9 Cyg 1 is $\log N(\mathrm{O})_{9\ \mathrm{Cyg}\ 1} = 8.74 \pm 0.10$, which coincides within the errors with the non-LTE solar abundance, $\log N(\mathrm{O})_\odot = 8.69 \pm 0.05$ [20], possibly indicating that non-LTE effects are

Table 5. Parameters and equivalent widths of FeII lines and the iron abundance in the atmosphere of 9 Cyg 1 derived from each line

λ, Å	ε_i, eV	$\log gf$	W_λ, mÅ	$\log N(\mathrm{Fe})$
4583.83	2.79	−1.87	205.7	7.45
4620.52	2.83	−3.29	85.5	7.15
5100.66	2.81	−4.17	61.0	7.60
5234.63	3.22	−2.27	123.4	7.10
5264.79	3.25	−3.23	78.6	7.37
5316.62	3.15	−1.85	246.8	7.93
5325.55	3.22	−3.32	80.8	7.46
5337.73	3.23	−3.89	77.1	8.00
5362.87	3.20	−2.74	157.3	8.02
5408.82	5.96	−2.39	4.9	7.21
5414.07	3.22	−3.54	55.9	7.26
5425.26	3.20	−3.16	65.7	7.05
5525.13	3.27	−3.94	43.1	7.52
5529.93	6.73	−1.88	22.9	8.31
5534.85	3.24	−2.73	117.7	7.48
6369.46	2.89	−4.16	53.2	7.51
6383.72	5.55	−2.27	39.1	8.03
6416.93	3.89	−2.85	81.3	7.69
6432.68	2.89	−3.52	73.4	7.18
6442.95	5.55	−2.89	10.1	7.78
6446.40	6.22	−1.96	17.0	7.80
6456.39	3.90	−2.10	109.2	7.37
6516.08	2.89	−3.32	95.7	7.31

Table 6. Model-atmosphere parameters for the Sun, Procyon A, and 9 Cyg 1

Star	T_{eff}, K	$\log g$	V_t, km/s	$\log N(\mathrm{C})_0$	$\log N(\mathrm{N})_0$	$\log N(\mathrm{O})_0$	$\log N(\mathrm{Fe})_0$
Sun	5770	4.40	1.00	8.39	7.78	8.66	7.45
Procyon A	6530	3.96	2.20	8.73	8.18	8.86	7.40
9 Cyg 1	5300	2.80	2.47	8.52	8.01	8.89	7.63

small for 9 Cyg 1 (the effective temperature of 9 Cyg 1 is lower than the solar value).

Our comparison of the observed and calculated spectra also enables confident estimation of the iron abundances in the atmospheres of the program stars:

$$\log N(\mathrm{Fe})_\odot = 7.43 \pm 0.05,$$
$$\log N(\mathrm{Fe})_{\alpha\,\mathrm{CMi}} = 7.44 \pm 0.05,$$
$$\log N(\mathrm{Fe})_{9\,\mathrm{Cyg}\,1} = 7.53 \pm 0.05.$$

We also estimated the abundances of other elements, presented in Tables 7–9 and Fig. 6, where we compare the atmospheric abundances of several elements for 9 Cyg 1, the Sun, and Procyon A. The abundances of all the elements essentially coincide, with the exception of C, N, and O.

The higher abundances of C, N, and O in the atmosphere of Procyon compared to the solar values could be due to neglected non-LTE effects, which should be stronger than for the Sun because of its higher effective temperature, as well as to effects associated with the evolution of the chemical composition in binaries [23–25].

4. EVOLUTIONARY STATUS OF 9 Cyg

To estimate the binary's combined luminosity, we must know its parallax. There are several parallax estimates in the literature, which lead to the combined luminosities $L/L_\odot = 201$ for $\pi = 0.00585''$ [4], $L/L_\odot = 182$ for $\pi = 0.00606''$ [10], and $L/L_\odot = 159$ for $\pi = 0.00641''$ [8]. As we noted above, the Hipparcos astrometric parallax of 9 Cyg [10] has an uncertainty of about 10% and overestimates the luminosities of the components. Therefore, we believe that the parallax $\pi = 0.00641''$, which differs from the Hipparcos value by less than 10%, is best available estimate. In this case, $L = 159\ L_\odot$, and the component luminosities are $L_1 = 103.8\ L_\odot$ and $L_2 =$

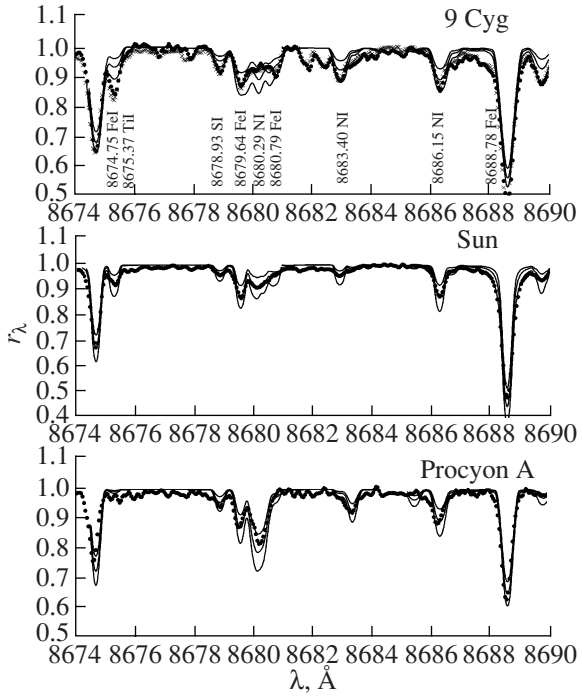

Fig. 4. Same as Fig. 3 for the NI lines.

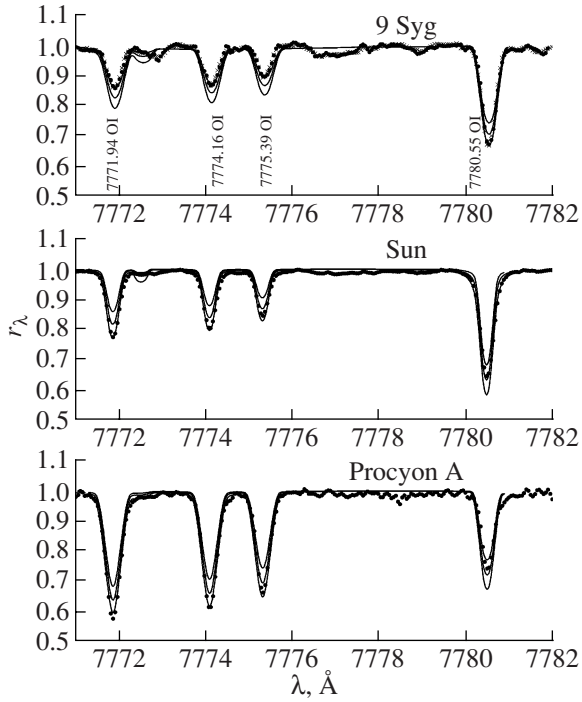

Fig. 5. Same as Fig. 3 for the OI lines.

Table 7. Line parameters for synthetic-spectrum computations in the region of CI lines

Ion	λ, Å	log gf	ε_i, eV	log $N_\odot$	log $N_{\alpha\,\mathrm{CMi}}$	log $N_{9\,\mathrm{Cyg}\,1}$
FeI	4930.32	−0.90	3.96	7.45	7.35	7.68
VI	4932.03	−0.87	1.22	4.26	4.11	4.06
CI	4932.05	−1.88	7.68	8.69	8.73	8.52
FeI	4933.29	−2.29	3.30	7.35	7.45	7.33
FeI	4934.01	−0.59	4.15	7.35	7.40	7.33
BaII	4934.08	−0.15	0.00	2.09	2.09	2.00
FeI	5049.82	−1.36	2.28	7.35	7.10	7.23
NiI	5051.51	−0.84	3.65	6.21	6.21	6.21
CI	5051.58	−2.48	8.54	8.24	8.43	8.22
FeI	5051.63	−2.80	0.92	7.30	7.40	7.23
CrI	5051.90	−2.98	0.94	5.63	5.33	5.63
CI	5052.17	−1.65	7.68	8.69	8.73	8.22
TiI	5052.87	−0.24	2.18	4.95	4.95	4.95
FeI	5052.97	−3.04	3.27	7.30	7.40	7.73
FeI	5379.57	−1.51	3.69	7.45	7.25	7.63
CI	5380.22	−2.03	8.85			
CI	5380.26	−2.82	8.85	8.39	8.60	8.22
CI	5380.34	−1.84	7.68			
TiII	5381.02	−1.67	1.57	4.95	4.65	4.95
CrI	5381.09	−4.06	4.45	5.63	5.33	5.63
CoI	5381.10	−2.37	1.96	4.88	4.73	4.88
FeI	5382.45	−1.06	4.37	7.30	7.40	7.58
FeI	5383.37	0.64	4.31	7.40	7.35	7.35
FeI	7108.38	−3.42	5.55	7.45	7.35	7.68
CI	7108.93	−1.59	8.64	8.69	8.53	8.32
NiI	7110.89	−2.98	1.94	6.21	6.21	6.21
CI	7111.47	−1.09	8.64	8.69	8.53	8.32
FeI	7112.18	−3.00	3.00	7.50	7.40	7.63
CI	7113.18	−0.77	8.65	8.39	8.43	8.22
FeI	7114.73	−2.38	5.45	7.45	7.40	7.63
CI	7115.17	−0.94	8.64	8.39	8.53	8.22
CI	7115.18	−1.47	8.64			

Table 8. Line parameters for synthetic-spectrum computations in the region of NI lines

Ion	λ, Å	log gf	ε_i, eV	log $N_\odot$	log $N_{\alpha\,\mathrm{CMi}}$	log $N_{9\,\mathrm{Cyg}\,1}$
FeI	8674.75	−1.80	2.83	7.45	7.50	7.72
TiI	8675.37	−1.37	1.07	4.95	4.50	<5.25
		−1.67				
SI	8678.93	−0.40	7.87	7.14	7.29	7.57
		−1.00				
SI	8679.72	−0.26	7.87	7.14	7.14	7.17
		−0.41				
FeI	8679.64	−1.15	4.97	7.45	7.40	7.63
		−1.45				
SiI	8680.08	−1.60	5.86	7.51	7.41	7.41
		−1.00				
NI	8680.29	0.35	10.34	7.78	8.08	8.01
SI	8680.41	−0.21	7.87	7.14	7.04	7.07
SiI	8680.55	−2.34	6.10	7.51	7.41	7.41
FeI	8680.79	−2.41	4.19	7.45	7.35	7.63
NI	8683.40	0.07	10.33	7.78	8.18	8.31
NI	8686.15	−0.30	10.33	7.78	8.18	8.31
FeI	8688.63	−1.51	2.18	7.35	7.55	7.63
		−1.21				

55.2 $L_\odot$. With these luminosities and our derived effective temperatures, the components fit the evolutionary isochrone [26] with $\log t = 8.60$ (where t is the evolutionary age in years) for stars with $z = 0.019$ and masses close to those estimated in [4]. The corresponding isochrones and positions of the components are presented in Fig. 7. It is not possible to place both components on the same isochrone with other luminosity and temperature combinations. Base on the general belief that, as a rule, the components of multiple systems have common origins and ages, we conclude that the binary's most probable luminosity is 159 $L_\odot$, so that the components' luminosities are $L_1 = 103.8\,L_\odot$ and $L_2 = 55.2\,L_\odot$, their effective temperatures $T_{eff\,1} = 5300$ K and $T_{eff\,2} = 9400$ K, and their masses $M_1 = 2.915\,M_\odot$ and $M_2 = 2.497\,M_\odot$.

Table 9. Line parameters for synthetic-spectrum calculations in the region of the OI lines

Ion	λ, Å	log gf	ε_i, eV	log $N_\odot$	log $N_{\alpha\,\mathrm{CMi}}$	log $N_{9\,\mathrm{Cyg}\,1}$
OI	7771.94	0.37	9.15	8.96	9.16	8.59
FeI	7772.60	−2.03	5.07	7.45	7.50	7.33
OI	7774.16	0.22	9.15	8.96	9.16	8.59
OI	7775.39	0.00	9.15	8.96	9.16	8.59
FeI	7780.55	−0.45	4.47	7.45	7.40	7.73
		−2.36				
SiI	8443.97	−1.40	5.87	7.61	7.51	7.51
OI	8446.25	−0.46	9.52	8.96	8.96	8.89
OI	8446.36	1.72	9.52	8.96	8.96	8.89
FeI	8446.39	−1.16	4.99	7.65	7.60	7.53
FeI	8446.57	−1.50	4.91	7.65	7.60	7.53
OI	8446.76	1.03	9.52	8.96	8.96	8.89

5. CONCLUSIONS

Thus, the components of the binary 9 Cyg have an age close to 400 million years, effective temperatures and surface gravities of $T_{eff} = 5300$ K, $\log g = 2.80$ for component 1 and $T_{eff} = 9400$ K, $\log g = 3.95$ for component 2. The radii implied by the masses and $\log g$ values are $R_1 = 11.2\ R_\odot$ and $R_2 = 2.8\ R_\odot$.

Hydrogen is completely depleted at the center of component 1, the core is in the process of contracting, and the star's envelope is expanding: the star is approaching the onset of core helium burning, but is still moving along the asymptotic giant branch. At the same time, component 2 is in the middle of its core hydrogen burning, and the star itself lies within the main-sequence strip.

Our data on the atmospheric abundances of 9 Cyg 1 are fairly accurate, as is confirmed by a comparison of our abundances for several elements for the Sun and Procyon A with those derived by other authors. Our iron abundances for the atmospheres of the Sun and Procyon A coincide with the most recent estimations of these parameters using the most refined techniques [27, 28]. The metallicity we find for 9 Cyg 1, [Fe] = +0.1, reflects the fact that, on average, 9 Cyg has solar chemical abundances.

On the other hand, the significant differences in the relative abundances of C and N in the atmospheres of 9 Cyg 1 and the Sun are probably due to mixing between the atmospheric material and matter from the region of nuclear reactions, where virtually all carbon is transformed into nitrogen during hydrogen burning in the CNO cycle. Such mixing, probably stimulated by binarity [23], occurred during this component's evolution near the main sequence, as well as its evolution towards the red-giant region. Thus, all the chemical-composition peculiarities of 9 Cyg 1 can be explained by evolutionary changes in the star itself.

Our self-consistent and fairly accurate estimation of the fundamental parameters of the components of

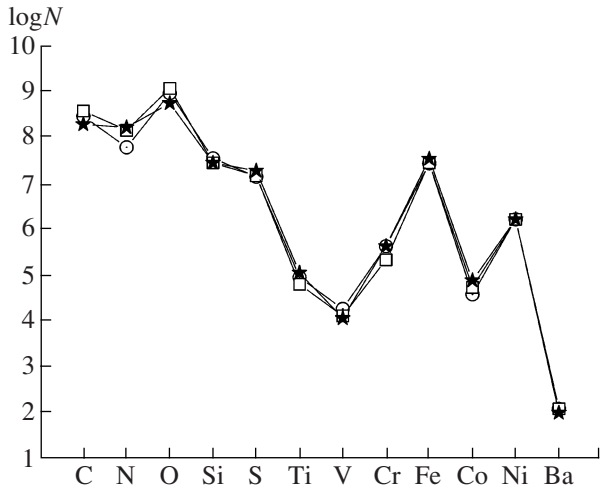

Fig. 6. Comparison of the atmospheric abundances of 9 Cyg 1 (asterisks), the Sun (circles), and Procyon A (squares).

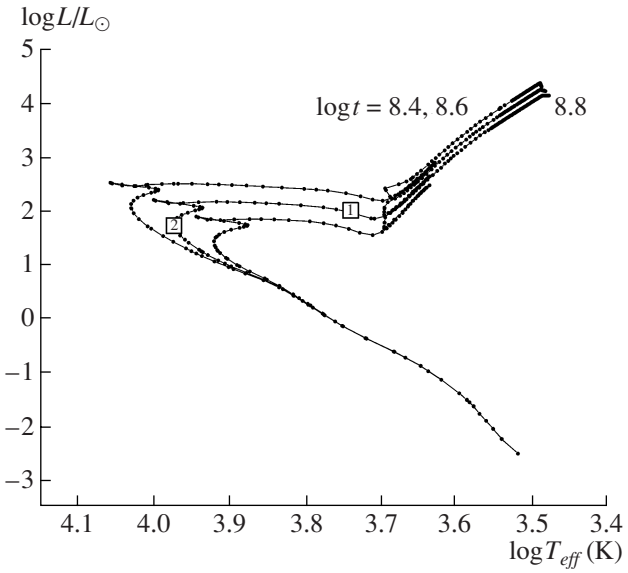

Fig. 7. Positions of the components of 9 Cyg on evolutionary-track isochrones. The sizes of the squares correspond to the rms uncertainties.

9 Cyg for our observation epochs enables us to draw some conclusions about the evolution of several parameters of the binary system. The fact that the components lie on a single evolutionary-track isochrone assures the accuracy of the component-mass estimates and enables us to estimate the parameters of the components at the onset of their main-sequence evolution. The initial radii derived by interpolating the evolutionary-track data [25] for the masses $M_1 = 2.915\ M_\odot$ and $M_2 = 2.497\ M_\odot$ are $R_1^0 = 1.89\ R_\odot$ and $R_2^0 = 1.75\ R_\odot$. Thus, the radii have increased approximately sixfold for component 1 and by a factor of 1.6 for component 2. If these radius increases occurred without mass loss by the system's components and with conservation of angular momentum, the initial rotational rates of the components were $v \sin i = 78$ km/s for component 1 and $v \sin i = 320$ km/s for component 2; the reason for this difference is not clear.

Our study shows that 9 Cyg has the following characteristic features.

1. The binary's age is 400 million years, and its orbit very eccentric: $e = 0.7887$.

2. Our abundance estimates provide evidence for mixing of matter in component 1 during its main-sequence evolution. Such mixing is possible for binaries with short periods near 50 days or shorter. At the same time, such mixing is improbable for systems with periods near 1500 days and longer [24], and currently 9 Cyg has precisely such a period.

3. The rotational rate inferred for component 2, 200 km/s, may indicate that the components' rotational rates at the onset of their evolution were rather high.

The problem of the high orbital eccentricity of 9 Cyg cannot be solved by assuming resonance-like processes that increase the eccentricity of the orbit: the star is only a binary, and the presence of a third body has not been established. At the same time, the considerable mixing we have inferred may testify that the binary's orbital parameters have changed, in the sense that the period and semi-major axis of its elliptical orbit have increased.

To explain these observations, we consider the following model. Let us suppose that, initially, the system consisted of components with rotational rates at the stability limit. For a mass of $3\ M_\odot$ and a radius of $R = 1.9\ R_\odot$ (the initial parameters of 9 Cyg 1), this rate is ∼540 km/s. This rate for 9 Cyg 2 ($M_2 = 2.5\ M_\odot$ and $R_2 = 1.75\ R_\odot$) is approximately the same at the same time: ∼520 km/s. If the system had a circular orbit with a radius equal to the current periastron distance, $r = a(1 - e) = 6 \times 10^7$ km, its period was about 50^d, providing conditions suitable for mixing. The mass distribution in the stars is not point-like, and gravity forms tidal bulges on each of star, which move faster than the companion in its orbit; this leads to an acceleration of the orbital motion, the energy for which comes from the axial rotational energy of the components.

To get an orbit with a semi-major axis of 3×10^8 km, an eccentricity of $e = 0.7887$, and a period of 1500^d, as is observed now [4], from an initially circular orbit, it is necessary to increase the binary's orbital energy, $E_{orb} = -GM_1M_2/2a$, by 1.33×10^{47} erg.

If a star with a mass of $3\ M_\odot$ and a radius of $R = 1.9\ R_\odot$ rotates at ∼540 km/s, its rotational energy is $E_{rot} = 0.2MR^2\omega^2 = 3.58 \times 10^{48}$ erg. The star's axial rotational period is $\sim 0.17^d$, considerably shorter than the orbital period. Thus, about 4% of the rotational energy of one of the components is sufficient for the initially circular orbit to evolve into a highly eccentric elliptical orbit. This mechanism for increasing the orbital period and semi-major axis does work, as is observed in the case of the increasing period and semi-major axis for the Moon's orbit around the Earth [29, 30].

Consequently, first, we conclude that an initially circular orbit can become elliptical in 400 million years. Second, the initially small orbital radius and short period ($<50^d$) can create conditions required for mixing. Third, the difference of the component masses gives rise to different mass distribution with radius, and so different rotational-energy loss rates; as a result, the rotational rate can currently be much higher for the lower-mass star (component 2) than for 9 Cyg 1.

REFERENCES

1. J. A. Hynek, Contrib. Perkins Obs. **191**, 1 (1938).
2. A. H. Markovitz, *A Study of Stars Exhibiting Composite Spectra* (Ohio State Univ., Columbus, 1969).
3. H. A. Abt and S. G. Levy, Astrophys. J., Suppl. Ser. **30**, 273 (1976).
4. R. Griffin, R. Griffin, and D. W. Beggs, Mon. Not. R. Astron. Soc. **270**, 409 (1994).
5. P. Baize, Astron. Astrophys., Suppl. Ser. **81**, 415 (1989).
6. M. Sheller, I. Balega, Yu. Balega, et al., Pis'ma Astron. Zh. **24**, 337 (1998) [Astron. Lett. **24**, 283 (1998)].
7. S. B. Parsons and T. B. Ake, Astrophys. J., Suppl. Ser. **119**, 83 (1998).
8. C. Martin, F. Mignard, W. I. Hartkopf, and H. A. McAlister, Astron. Astrophys., Suppl. Ser. **133**, 149 (1998).
9. N. Ginestet and J. M. Carquillat, Astrophys. J., Suppl. Ser. **143**, 513 (2002).
10. *The Hipparcos and Tycho Catalogues*, ESA SP-1200 (European Space Agency, 1997).

11. T. Schmidt-Kaler, K. Schaifers, in *Numerical Data and Functional Relationships in Science and Technology. New Series. Group 6. Astronomy and Astrophysics. V. 2b. Stars and Star Clusters*, Ed. by K. Landolt-Bornstein and H. H. Voigt (Springer, Berlin, 1982).
12. F. A. Musaev, G. A. Galazutdinov, A. V. Sergeev, et al., Kinematika Fiz. Nebesnykh Tel **15** (3), 282 (1999).
13. G. A. Galazutdinov, htp://ftp.sao.ru (2002).
14. V. V. Tsimbal, private communiction (2002).
15. D. Shulyak, V. Tsymbal, T. Ryabchikova, et al., Astron. Astrophys. **428**, 993 (2004).
16. V. V. Leushin and G. P. Topil'skaya, Astrofizika **22**, 121 (1985) [Astrophys. **22**, 74 (1985)].
17. N. Grevesse and A. J. Sauval, Astron. Astrophys. **347**, 348 (1999).
18. F. Kupka, N. E. Piskunov, T.A. Ryabchikova, et al., Astron. Astrophys., Suppl. Ser. **138**, 119 (1999).
19. Yu. Yu. Balega, V. V. Leushin, and G. Vaĭgel't, Astron. Rep. **49**, 217 (2005).
20. K. Lodders, Astrophys. J. **591**, 1220 (2003).
21. E. Anders and N. Grevesse, Geochim. Cosmochim. Acta **53**, 197 (1989).
22. M. Asplund, N. Grevesse, A. J. Sauval, et al., Astron. Astrophys. **417**, 75 (2004).
23. V. V. Leushin, Kinematika Fiz. Nebesnykh Tel **5** (5), 47 (1989).
24. Yu. Yu. Balega, V. V. Leushin, and M. K. Kuznetsov, Astron. Zh. **82**, 1099 (2005) [Astron. Rep. **49**, 984 (2005)].
25. V. V. Leushin, V. A. Urpin, and D. G. Yakovlev, Pis'ma Astron. Zh. **15**, 1008 (1989) [Astron. Lett. **15**, 439 (1989)].
26. L. Girardi, A. Bressan, G. Bertelli, and C. Chiosi, Astron. Astrophys., Suppl. Ser. **141**, 371 (2000).
27. M. Asplund, A. Nordlund, R. Trampedach, and R. E. Stein, Astron. Astrophys. **359**, 743 (2000).
28. C. Allende Prieto, M. Asplund, R. J. G. Lopez, and D. L. Lambert, Astrophys. J. **567**, 544 (2002).
29. O. Struve, B. Lynds, and H. Pillans, *Elementary Astronomy* (Oxford Univ. Press, New York, 1959).
30. J. Chapront and M. Chapront-Touze, Celest. Mech. **66**, 31 (1997).

Translated by N. Samus'